



Micro-electro-mechanically tunable metamaterial with enhanced electro-optic performance

Prakash Pitchappa, Chong Pei Ho, Yu-Sheng Lin, Piotr Kropelnicki, Chia-Yi Huang, Navab Singh, and Chengkuo Lee

Citation: *Applied Physics Letters* **104**, 151104 (2014); doi: 10.1063/1.4871517

View online: <http://dx.doi.org/10.1063/1.4871517>

View Table of Contents: <http://scitation.aip.org/content/aip/journal/apl/104/15?ver=pdfcov>

Published by the [AIP Publishing](#)

Articles you may be interested in

[Mechanism of the linear electro-optic effect in potassium dihydrogen phosphate crystals](#)

J. Appl. Phys. **104**, 073116 (2008); 10.1063/1.2990769

[Intrinsic optical modulation mechanism in electro-optic crystals](#)

Appl. Phys. Lett. **92**, 221111 (2008); 10.1063/1.2940340

[Near-resonance electro-optic activity enhancement and improved modulation performance for polymer based Fabry–Pérot interferometers](#)

Appl. Phys. Lett. **92**, 203302 (2008); 10.1063/1.2931086

[Enhanced electro-optic response of layered composite materials](#)

Appl. Phys. Lett. **74**, 2417 (1999); 10.1063/1.123866

[Enhancement of electro-optical performance in nematic emulsion films](#)

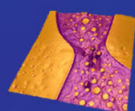
J. Appl. Phys. **85**, 2894 (1999); 10.1063/1.369053

Asylum Research Atomic Force Microscopes

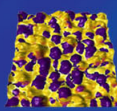
Unmatched Performance, Versatility and Support



The Business of Science®

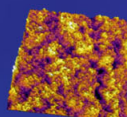


Modulus of Polymers
& Advanced Materials



Piezoelectrics
& Ferroelectrics

Coating Uniformity
& Roughness



Nanoscale Conductivity
& Permittivity Mapping



+1 (805) 696-6466
sales@AsylumResearch.com
www.AsylumResearch.com

Micro-electro-mechanically tunable metamaterial with enhanced electro-optic performance

Prakash Pitchappa,^{1,2} Chong Pei Ho,^{1,2} Yu-Sheng Lin,¹ Piotr Kropelnicki,^{2,a)} Chia-Yi Huang,³ Navab Singh,² and Chengkuo Lee^{1,b)}

¹Department of Electrical and Computer Engineering, National University of Singapore, 4 Engineering Drive 3, Singapore 117576

²Institute of Microelectronics (IME), 11 Science Park Road, Singapore 117685

³Department of Applied Physics, Tunghai University, No. 1727, Sec. 4, Taiwan Boulevard, Taichung 40704, Taiwan

(Received 17 February 2014; accepted 4 April 2014; published online 15 April 2014)

We experimentally demonstrate a micro-electro-mechanically tunable metamaterial with enhanced electro-optical performance by increasing the number of movable cantilevers in the symmetrical split ring resonator metamaterial unit cell. Simulations were carried out to understand the interaction of the incident terahertz radiation with out-of-plane deforming metamaterial resonator. In order to improve the overall device performance, the number of released cantilever in a unit cell was increased from one to two, and it was seen that the tunable range was doubled and the switching contrast improved by a factor of around five at 0.7 THz. This simple design approach can be adopted for a wide range of high performance electro-optical devices such as continuously tunable filters, modulators, and electro-optic switches to enable future photonic circuit applications. © 2014 AIP Publishing LLC. [<http://dx.doi.org/10.1063/1.4871517>]

Electromagnetic (EM) metamaterial is an array of sub-wavelength structures engineered to achieve material properties that usually does not exist in nature, such as negative refractive index,^{1,2} perfect absorption,^{3–5} and sub-wavelength focusing.^{6,7} Owing to these exotic properties, metamaterials has become an ideal candidate for a wide range of promising applications, such as optical cloaking,^{8,9} perfect absorbers,^{3–5} and super resolution imaging.^{6,7} These extreme electromagnetic properties are achieved through the interaction of the incident electromagnetic wave with the designed metamaterial pattern shape and size. Hence, by changing the metamaterial pattern shape through external stimulus, the interaction of the EM wave can be actively controlled. Various mechanisms are used for external control such as optical,¹⁰ electrical,¹¹ mechanical,¹² thermal,¹³ and magnetic.¹⁴ Most of these approaches use exotic materials, adopt complex fabrication processes, or demand bulky setup for providing external control. Very recently, Micro-electro-mechanical systems (MEMS) based actively tunable metamaterials have been reported either using electrostatic comb drive^{15–17} or released cantilevers as micro-actuators in the metamaterial unit cell^{18–21} to change the metamaterial pattern dimension. Electrostatic comb drive provides a wider tuning range and better switching contrast; however, they are usually slower and are not suitable for high frequency modulators owing to their larger moving mass. On the other hand, MEMS cantilevers provide an alternative approach, which is more suitable for high speed applications, but due to the limited actuation distance between the released cantilever and substrate, the tuning range and switching contrast is usually lower. In order to increase the electro-optical performance,

the actuation distance can be increased, but this will adversely affect the actuation voltage needed for tuning the cantilever over the increased gap.

In this paper, we have experimentally demonstrated a design approach to overcome the tradeoff between the limitation of tunability or switching contrast and actuation voltage in MEMS metamaterial, by utilizing multiple movable cantilevers in a single metamaterial unit cell for terahertz (THz) spectral range. In order to comprehensively validate the proposed design approach, symmetrical split ring resonator (SSRR) with increased number of movable cantilevers in the unit cell is considered. The proposed design approach can be adopted for a wide range of electro-optic devices, including THz filters, modulators, absorbers, and optical switches, without adversely affecting the actuation voltage, device footprint, and fabrication complexity of the devices.

The metamaterial pattern for the MEMS tunable metamaterial is a SSRR with two released cantilevers is shown in Fig. 1(a). It consists of 100×100 array of unit cell with pitch, P , of $120 \mu\text{m}$. The SSRR metamaterial pattern is designed to have four geometrically identical cantilevers. Two of these cantilevers (C_A and C_B) are released and can be actuated in out-of-plane direction, independently and other two cantilevers are fixed to the substrate (C_C and C_D) as shown in Fig. 1(a). The cantilever length (bl), tip length (tl), and width (bw) of each cantilever are $40 \mu\text{m}$, $20 \mu\text{m}$, and $3 \mu\text{m}$, respectively, as shown in Fig. 1(b). The in-plane gap between the tip of cantilever and corner structure, g_i , is $3 \mu\text{m}$. The cantilevers are made of $0.5 \mu\text{m}$ thick aluminum (Al) with a 40 nm aluminum oxide (Al_2O_3) dielectric layer, fabricated on a silicon substrate using standard complementary metal oxide semiconductor compatible process.¹⁸ Fig. 1(a) shows the SEM image of the fabricated MEMS tunable THz metamaterial unit cell with two released and unreleased cantilevers each. After the release process, the

^{a)}Currently address: Excelitas Technologies, 8 Tractor Rd., Singapore 627969.

^{b)}Author to whom correspondence should be addressed. Electronic mail: elelc@nus.edu.sg

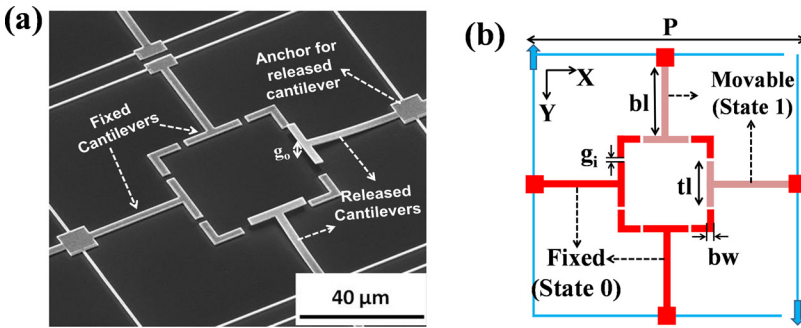


FIG. 1. (a) SEM image of fabricated symmetrical split ring resonator unit cell with two movable and two fixed cantilevers, and (b) Top view schematics for the unit cell shown in (a) with the geometrical pattern definitions.

bimaterial cantilevers are bend up due to residual stress in the structural layers (Al and Al_2O_3), thereby increasing the air gap between the released cantilever and Si substrate, i.e., g_o of about $15\ \mu\text{m}$. In order to achieve active tuning, electrostatic actuation mechanism was used by applying voltage across the released cantilever and Si substrate. As the voltage is increased between the released cantilever and Si substrate, the out-of-plane air gap, g_o , will reduce until there is no more air gap beneath the released cantilever.¹⁸ For simplicity, the state in which the cantilever is bent up is termed as state “1” (S1), while state “0” (S0) refers to the case where there is no air gap between the cantilever and Si substrate. State “0” can occur either due to the complete actuation of released cantilever to the substrate or the cantilevers are not released, thereby making it fixed to the substrate at all times.

To investigate the enhancement in tunable range for metamaterial using multiple movable cantilevers, the device was characterized in three configurations. In the first configuration, no actuation voltage is applied, so two cantilevers are in state S0 and two in state S1. In second configuration, actuation voltage is applied to one of the two movable cantilevers and other is unactuated, so one of the cantilevers is in state S1 and three in S0 state. In the third configuration, actuation voltage is applied to both the movable cantilevers, so all four cantilevers are in S0 state. In order to understand the resonant behavior of the SSRR structure in different configurations and analyze the effect of tuning air gap, with respect to the incident THz radiation, finite difference time domain (FDTD) modeling was carried out. Figure 2(a) shows the device in third configuration with all four cantilevers at S0 state and is used to explore the resonant mechanism of the planar SSRR metamaterial structure. The electric field of incident THz radiation (E_i) along X- and Y-direction is considered as TE and TM mode, respectively. For the simulation, the TE incidence is considered, and the scattered E_Y and E_Z fields on the metamaterial surface for the third device configuration is shown in Figs. 2(b) and 2(c), respectively. The anti-parallel currents induced in the SSRR structure in Fig. 2(b) clearly indicate the electrically induced magnetic resonance in the metamaterial structure. It can also be seen that there is an E_Z field induced between the cantilevers and substrate as shown in Fig. 2(c). To further understand the effect of changing air gap on the resonant behaviors of the SSRR structure, the device in first configuration with two released cantilevers (C_A and C_B) as shown in Fig. 2(d) is simulated. For TE incidence, the induced E_Y field along the C_D tip is same as in the previous case, where all the cantilevers are in S0 state. But unlike the earlier case, there is no E_Y field induced in the

released cantilever, C_B , as shown in Fig. 2(e). There is also a strong E_Z field coupled to the air gap region between both the released cantilevers (C_A and C_B) and Si substrate irrespective of polarization of the incident THz radiation, as shown in Fig. 2(f). From simulation results, it is clear that for out-of-plane actuated cantilevers based MEMS metamaterial, the primary variable parameter that strongly influences the resonant frequency is the out-of-plane capacitance (C_{OA} and C_{OB}) between the released cantilevers and Si substrate. The magnetic resonance of SSRR metamaterial structure can be considered as a LC model, and the resonant frequency of the LC model is given by $\omega_r = 1/\sqrt{L_{\text{eff}}C_{\text{eff}}}$, where L_{eff} and C_{eff} are the overall effective inductance and capacitance of the circuit.^{22,23} This simplified LC model can be used to qualitatively explain the experimental data in the following paragraph.

For characterization of different configurations of the devices, transmission spectra were measured using Terahertz

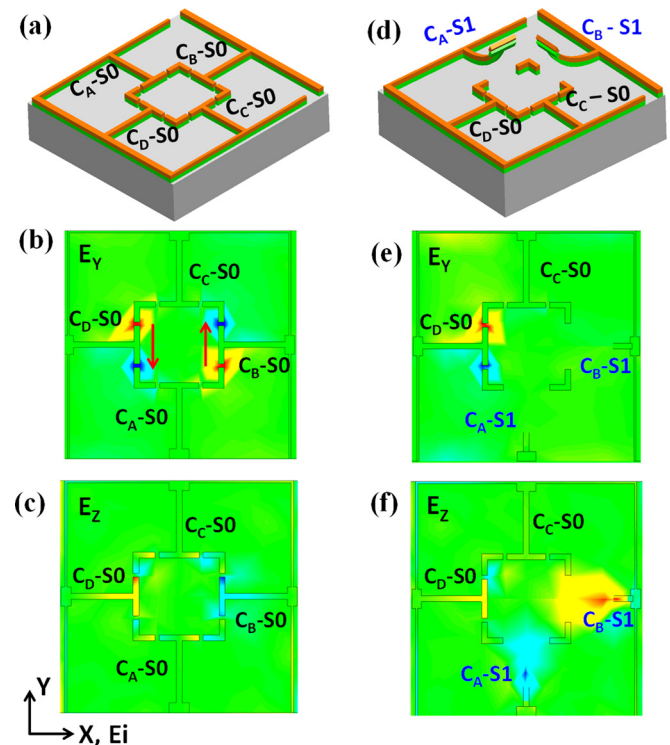


FIG. 2. (a) Schematics of the tunable metamaterial in third configuration with all cantilevers in state S0. (b) Y- and (c) Z-component of the scattered electric field, respectively, for TE incidence on device configuration shown in (a). (d) Schematics of the tunable metamaterial in first configuration with two cantilevers in state S1 (C_A and C_B) and two cantilevers in state S0 (C_C and C_D). (e) Y- and (f) Z-component of the scattered electric field, respectively, for TE incidence on device configuration shown in (d).

time-domain spectroscopy (THz-TDS) system over the THz range of 0.3–1 THz and were normalized to the free space transmission. To systematically characterize the devices at TE and TM incidence, two set of measurement were made, one by continuously actuating one of the released cantilever, while other is unactuated and in the other case, both the released cantilevers are actuated continuously. In order to facilitate the voltage input for the MEMS tunable metamaterial device, the fabricated devices were released using vapor hydrofluoric acid. Then, the released devices were wire-bonded onto a printed circuit board (PCB) with a center hole that allow the transmission of THz signal during THz-TDS testing. The entire chip size was $1\text{ cm} \times 1\text{ cm}$. Three bond-wire connections are made for actuation of cantilever C_A , actuation of cantilever C_B , and the Si substrate, which will act as ground. Since the electrical connections are separated between cantilever C_A and C_B , they can be actuated independently. The PCB with the THz MEMS metamaterial is held in position by a holder and THz signal was incident normally to the surface after passing through a polarizer, which controls the polarization of incident THz signal as shown in Fig. 3(a). All the measurements were carried out in nitrogen environment and Si substrate was used as the transmission reference. The transmission measurement was made by applying different voltages to cantilevers, C_A and C_B at TE and TM mode of incidence. Figure 4(a) shows the transmission spectra for TE incidence at different actuation voltage from 0 V to 25 V in steps of 5 V, applied across the cantilever, C_B and Si substrate. When there is no voltage applied to any cantilever, a resonant frequency dip is observed at 0.69 THz and the resonant frequency red shifts to 0.515 THz on increasing the actuation voltage to 25 V. For single cantilever actuation and TE incidence, the corresponding resonant frequency shift is about 0.175 THz. This can be qualitatively understood using the equivalent LC model as follows: when the actuation voltage is increased, the out-of-plane air gap

decreases, causing the corresponding out-of-plane capacitance, C_{OB} , to increase, which results in the red shift of the resonant frequency as seen from the measurement data in Fig. 4(a). More interesting, in case of TM incidence, a similar red shift in resonant frequency is observed from 0.71 THz to 0.54 THz for an increase in actuation voltage from 0 V to 25 V for same single cantilever actuation (C_B) as shown in Fig. 4(b). This is caused due to the strong coupling of E_z field in both the released cantilevers C_A and C_B at TE incidence as shown in Fig. 2(f). Therefore, irrespective of the cantilever actuated or polarization of the incident THz radiation, the resonant frequency will redshift with increasing actuation voltage. However, at TE incidence, the intensity of induced E_z field in the air gap under the cantilever C_A is slightly lower than C_B , and should be the reason for the slight reduction in tuning range between TE (0.175 THz) and TM (0.17 THz) mode of THz incidence.

For the second configuration of the device testing, where both the cantilevers are actuated at the same time by applying voltage of 0 V to 25 V, the resonant frequency shifts from 0.65 THz to 0.35 THz for both TE and TM incidence as shown in Figs. 4(c) and 4(d), respectively. The tuning range is around 0.3 THz, which is almost double compared to the case of single cantilever actuation. When both the cantilevers are actuated, capacitance due to both cantilevers and the Si substrate, C_{OA} and C_{OB} , decreases. Therefore, the overall capacitance change is amplified by approximately two-fold and so does the spectral shift in the resonant frequency for the case of two cantilever actuation. Additionally, when both the cantilevers are actuated, the effect of tuning will be the same for the TE and TM polarization of the incident radiation. Hence, by adopting this simple design principle of utilizing multiple released MEMS cantilevers in a SSRR configuration, the tuning range of the device can be doubled under the same actuation voltage. It can be seen that there is a slight difference in the initial resonant frequency value at 0 V, and

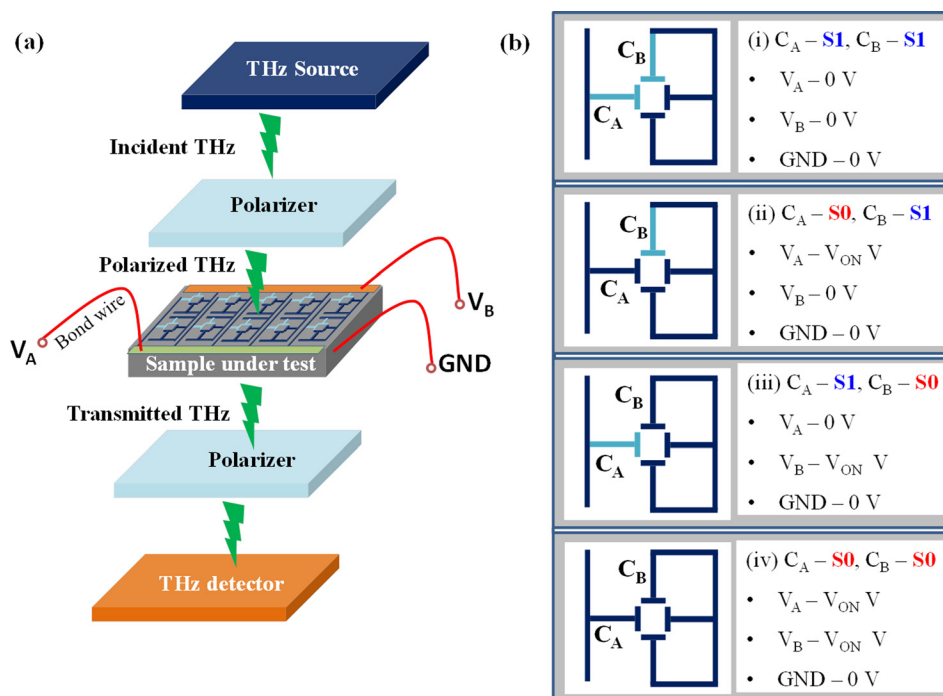


FIG. 3. (a) Schematics of experimental setup for THz transmission testing at different actuation voltage and (b) shows the four device configurations by applying different voltage combination for the two released cantilevers, C_A and C_B .

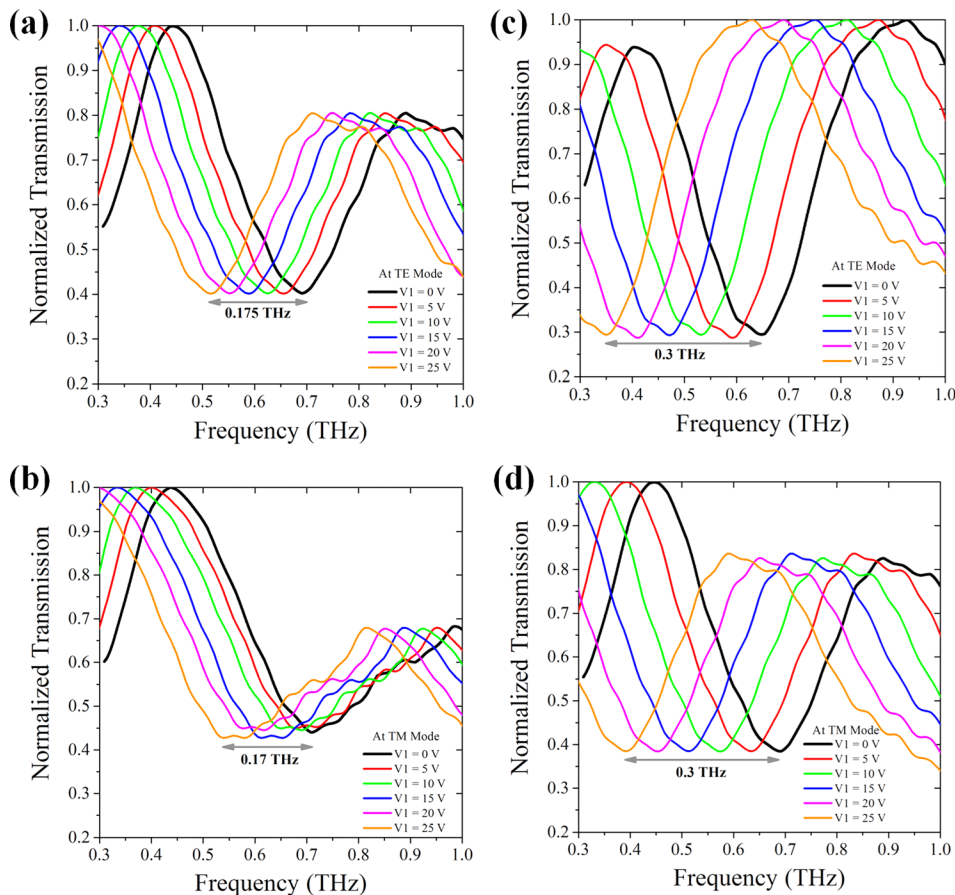


FIG. 4. Measured transmission spectra at various actuation voltages from 0 V to 25 V in steps of 5 V for TE incidence (E_i field along X- direction) with (a) one cantilever (C_B) actuated and (c) two cantilevers (C_A and C_B) actuated, respectively. Measured transmission spectra at various actuation voltages from 0 V to 25 V in steps of 5 V for TM incidence (E_i field along Y-direction) with (b) one cantilever (C_B) actuated and (d) two cantilevers (C_A and C_B) actuated, respectively.

may be attributed to the variation of release height of the bimaterial cantilevers and the difference in measurement spectra for TE and TM mode may be caused due to the non-symmetry in the routing metal lines along X and Y directions.

In order to further explore the impact of the proposed scheme in application level performance, the tunable metamaterial was also characterized as an electro-optic switch. The key performance parameter for an electro-optic switch is to have a striking switching contrast, which is described as $SC = (T_{20} - T_0) / T_0$, where T_0 and T_{20} is the transmission spectra at 0 V and 20 V, respectively.²⁴ In order to characterize the performance improvement of the metamaterial device as a switch, three sets of transmission spectra measurement were made—(1) Initial condition: C_A and C_B in state S1 and C_C and C_D in state S0, (2) single cantilever actuated: C_A in state S1 and C_B , C_C and C_D in state S0, and (3) both cantilevers actuated: C_A , C_B , C_C , and C_D in state S0. The transmission spectra for the single cantilever actuation and two cantilevers actuation at 0 V and 20 V for TE incidence are measured. The switching contrast is then calculated for these two cases, as shown in Fig. 5, where the grey and red region show the switching contrast of single and two cantilevers actuation, respectively. It can be seen that the switching contrast for the two cantilever actuated case is enhanced over the major portion of the spectral range compared to the single cantilever actuation. A maximum enhancement of around 5 times in switching contrast is achieved at 0.7 THz. The proposed approach of utilizing multiple cantilevers to achieve enhanced electro-optic performance can be further

re-designed for any spectral region of interest without affecting the device footprint, actuation voltage, material selection, and the process complexity.

In summary, we investigated and demonstrated a design approach of using multiple MEMS cantilevers to improve the overall electro-optic performance, such as tunability and switching contrast, without adversely affecting the size, actuation voltage, and complexity of the fabrication process. It was experimentally verified that the tuning range was

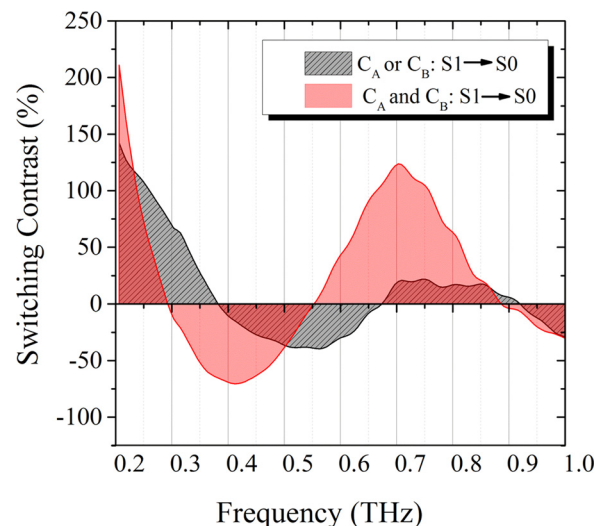


FIG. 5. Electro-optic switching contrast for MEMS tunable metamaterial with single cantilever actuation (grey-crossed region) and two cantilever actuation (red-shaded region).

doubled, when the number of cantilevers actuated was increased from one to two. The device was also characterized as an electro-optic switch, which shows a maximum enhancement in switching contrast of about 5 times achieved at 0.7 THz for two cantilevers actuation. This simple design principle is of great value to achieve enhanced electro-optic characteristics and is completely scalable to any electromagnetic spectral region of interest. This approach can enable high performance, continuously tunable, optical devices ranging from sensors, filters, modulators to the striking electro-optic switches for future photonic circuit applications.

The authors acknowledge the financial support from research Grant No. AcRF Tier 2 - MOE2012-T2-2-154 at the National University of Singapore.

¹R. A. Shelby, D. R. Smith, and S. Schultz, *Science* **292**, 77 (2001).

²C. M. Soukoulis, S. Linden, and M. Wegener, *Science* **315**, 47 (2007).

³N. Landy, S. Sajuyigbe, J. Mock, D. Smith, and W. Padilla, *Phys. Rev. Lett.* **100**, 207402 (2008).

⁴N. Liu, M. Mesch, T. Weiss, M. Hentschel, and H. Giessen, *Nano Lett.* **10**, 2342 (2010).

⁵C. M. Watts, X. Liu, and W. J. Padilla, *Adv. Mater.* **24**, OP98 (2012).

⁶N. Fang, H. Lee, C. Sun, and X. Zhang, *Science* **308**, 534 (2005).

⁷X. Zhang and Z. Liu, *Nature Mater.* **7**, 435 (2008).

⁸D. Schurig, J. Mock, B. Justice, S. A. Cummer, J. Pendry, A. Starr, and D. Smith, *Science* **314**, 977 (2006).

⁹J. B. Pendry, D. Schurig, and D. R. Smith, *Science* **312**, 1780 (2006).

¹⁰H.-T. Chen, J. F. O'Hara, A. K. Azad, A. J. Taylor, R. D. Averitt, D. B. Shrekenhamer, and W. J. Padilla, *Nat. Photonics* **2**, 295 (2008).

¹¹H.-T. Chen, W. J. Padilla, J. M. Zide, A. C. Gossard, A. J. Taylor, and R. D. Averitt, *Nature* **444**, 597 (2006).

¹²I. M. Pryce, K. Aydin, Y. A. Kelaita, R. M. Briggs, and H. A. Atwater, *Nano Lett.* **10**, 4222 (2010).

¹³H. Tao, A. Strikwerda, K. Fan, W. Padilla, X. Zhang, and R. Averitt, *Phys. Rev. Lett.* **103**, 147401 (2009).

¹⁴Y. Poo, R. X. Wu, G. H. He, P. Chen, J. Xu, and R. F. Chen, *Appl. Phys. Lett.* **96**, 161902 (2010).

¹⁵W. M. Zhu, A. Q. Liu, X. M. Zhang, D. P. Tsai, T. Bourouina, J. H. Teng, X. H. Zhang, H. C. Guo, H. Tanoto, and T. Mei, *Adv. Mater.* **23**, 1792 (2011).

¹⁶W. M. Zhu, A. Q. Liu, T. Bourouina, D. P. Tsai, J. H. Teng, X. H. Zhang, G. Q. Lo, D. L. Kwong, and N. I. Zheludev, *Nat. Commun.* **3**, 1274 (2012).

¹⁷W. M. Zhu, A. Q. Liu, W. Zhang, J. F. Tao, T. Bourouina, J. H. Teng, X. H. Zhang, Q. Y. Wu, H. Tanoto, H. C. Guo, G. Q. Lo, and D. L. Kwong, *Appl. Phys. Lett.* **99**, 221102 (2011).

¹⁸Y.-S. Lin, Y. Qian, F. Ma, Z. Liu, P. Kropelnicki, and C. Lee, *Appl. Phys. Lett.* **102**, 111908 (2013).

¹⁹F. Ma, Y. Qian, Y.-S. Lin, H. Liu, X. Zhang, Z. Liu, J. M.-L. Tsai, and C. Lee, *Appl. Phys. Lett.* **102**, 161912 (2013).

²⁰Y.-S. Lin, F. Ma, and C. Lee, *Opt. Lett.* **38**, 3126 (2013).

²¹F. Hu, Y. Qian, Z. Li, J. Niu, K. Nie, X. Xiong, W. Zhang, and Z. Peng, *J. Opt.* **15**, 055101 (2013).

²²J. Zhou, E. N. Economon, T. Koschny, and C. M. Soukoulis, *Opt. Lett.* **31**, 3620 (2006).

²³Y. Pang, H. Cheng, Y. Zhou, and J. Wang, *J. Appl. Phys.* **113**, 114902 (2013).

²⁴J.-Y. Ou, E. Plum, J. Zhang, and N. I. Zheludev, *Nat. Nanotechnol.* **8**, 252 (2013).